Determination of Atrial Myofibre Orientation Using Structure Tensor Analysis for Biophysical Modelling

Marta Varela[1,⋆], Jichao Zhao[2], and Oleg V. Aslanidi[1]

[1] Biomedical Engineering, Division of Imaging Sciences, King's College London, UK
[2] Bioengineering Institute, University of Auckland, New Zealand
marta.varela@kcl.ac.uk

Abstract. Myofibre orientation plays an important role in electrical activation patterns in the heart. Biophysical models of the whole atria, however, have not yet incorporated realistic myofibre architecture. In this study, we use structure tensor (ST) analysis to determine myofibre orientation from high resolution micro-computed tomography (micro-CT) images and investigate the role of different ST image processing parameters on the computed fibre orientation fields. We found that, although some parameter sets can lead to non-physiological over- or under-smooth fibre fields, a wide range of values produced atrial fibre orientations that are in good agreement with previous anatomical and histological studies. The computed fibre fields can be incorporated in realistic 3D electrophysiological simulations to study electrical propagation under physiological and pathological conditions in the entire atria.

Keywords: cardiac fibre orientation, structure tensor, atrial fibrillation, biophysical modelling.

1 Introduction

Atrial fibrillation (AF) is a disturbance in the rhythm of the heart, characterised by rapid and disorganised activation of the atria. Despite its major health and socio-economic impact, the mechanisms underlying AF and the effects of different treatment options are still incompletely understood [1]. AF is the result of the complex interplay of several factors, ranging from alterations in cellular ion channels to structural remodelling of the atrial muscle. Computational models of the atria can integrate such multi-scale and multi-modal information, making them a valuable tool in the investigation of the mechanisms of AF.

Atrial muscle is highly anisotropic, with several major well-aligned myofibre bundles (such as the crista terminalis and the pectinate muscles (PMs) in the right atrium [2]) coexisting with highly complex and disorganised fibre arrangements in the pulmonary vein (PV) sleeves and surrounding left atrial tissue [3], where high frequency activity in AF commonly originates. As the conduction

⋆ Corresponding Author.

S. Ourselin, D. Rueckert, and N. Smith (Eds.): FIMH 2013, LNCS 7945, pp. 425–432, 2013.

of electrical signals in the myocardium occurs preferentially along muscular fibres, myofibre orientation plays a crucial role in determining the dynamics of action potential propagation in both physiological and pathological conditions. Computational 3D whole-atria models, however, have not incorporated realistic atrial myofibre architecture, using instead geometries with isotropic myofibre directions [4] or rule-based anisotropic fibres in some regions of the atria [5,6].

In this study, we show how a realistic model of atrial myofibre orientation can be built from high-resolution contrast micro-CT images using structure tensor (ST) analysis. We investigate the effect of varying ST image processing parameters on the fibre orientation field and compare the reconstructed myofibre architecture with previous anatomical and histological studies.

2 Methods

Image Acquisition

Canine atria were imaged *ex-vivo* using high-resolution micro-CT [7] and reconstructed to an isotropic resolution of 144 μm. The atria were incubated in an iodine solution prior to scanning, to allow iodine to accumulate in muscular tissue. This makes myocardial muscular fibres hyperintense in relation to surrounding connective tissue, allowing both tissue types to be easily distinguished in the acquired high-resolution images [8].

Fibre Orientation Computation

Structure tensor analysis [9] was used to determine the orientation of the myofibres from the 3D micro-CT intensity dataset.

Firstly, an isotropic 3D Gaussian filter (standard deviation, ρ, kernel size: m) is applied to the image to reduce the effect of noise. The derivatives of the image intensity along each direction: D_x, D_y, D_z, are then computed on a voxel-by-voxel basis by convolving the image with a Sobel-type Scharr operator [10], which computes the central difference in the direction of the derivative, whilst ensuring further smoothing in the perpendicular directions. The ST is then built for each voxel as the product of the computed derivatives:

$$ST = \begin{bmatrix} D_x * D_x & D_x * D_y & D_x * D_z \\ D_y * D_x & D_y * D_y & D_y * D_z \\ D_z * D_x & D_z * D_y & D_z * D_z \end{bmatrix} \quad (1)$$

Each element of the ST is further smoothed using another Gaussian filter (standard deviation, σ, kernel size: m), so that the ST reflects the orientation of the field in a neighbourhood of the voxel. Finally, eigendecomposition is applied to the ST to determine the eigenvector, v, paired with the lowest magnitude eigenvalue. For each voxel, the vector v corresponds to the direction along which the image intensity gradient varies the least and can be interpreted as the main direction of the myofibre in the voxel [11].

Choice of Image Processing Parameters

Although it is well know that σ is related to the noise scale of the image and ρ to the characteristic size of the image texture [9], there is no rigorous framework to determine the degree of smoothing that should be performed during ST calculations. We therefore varied σ, ρ and m over a wide range of values (σ, ρ: 0.1 to 12 and m: 3 to 50) to estimate the effect of these parameters on the reconstructed fibre field and determine an optimal set of parameters to be used in subsequent analyses and computational model development. Images were also postprocessed to investigate the effect of voxel size (altered from 144 μm to 72, 288 and 512 μm) and signal to noise ratio, SNR, through the addition of Gaussian noise with zero mean and a variable standard deviation. The estimated SNR of the images was altered from 132 to 25, 2.5 and 0.25.

Validation of the determined fibre orientation is difficult due to the lack of a gold standard model or existing comparable data. In agreement with anatomical descriptions [2,12], myofibres in well-defined atrial bundles (such as the PMs) were assumed to be aligned with the main bundle direction. In assessing the effect of smoothing parameters, two other reasonable assumptions were made: (i) parameters that give anatomically realistic fibre orientations in these well-defined bundles of varying size and geometry are also suitable in other atrial regions, (ii) optimal parameters do not allow for myofibre directions to end abruptly at free boundaries of cardiac tissue, i.e. their orientation does not have a component normal to the tissue surface.

After optimal ST smoothing parameters were chosen, we characterised fibre orientation across the atria, particularly in the myocardial sleeves of the PVs and the left atrial regions adjacent to them, where fibres are known to follow a complicated arrangement [3,13,14]. Fibre tracks were visualised as streamlines using Paraview 3.14.1 (Kitware, Clifton Park, NY, USA).

3 Results

Impact of Parameters on Reconstructed Fibre Fields

The effect of the used smoothing parameters can clearly be seen in the obtained fibre fields. Figure 1 shows, for example values of ρ, σ and m, the fibre field in the PM region, where myofibres are known to be mostly aligned with the main direction of each of the multiple bundles. The dependence of the fibre direction on the image processing parameters can be further appreciated by observing, in Figure 1, the main fibre orientation field in an approximately cylindrical portion of the PMs (middle row) and the corresponding histograms of the angle, α, between the computed fibre orientation vector in each voxel and the approximate axis of the cylindrical portion of the PM (bottom row).

For low smoothing values (e.g. $\rho = 0.1, \sigma = 0.1, m = 3$), fibre orientations point in more random directions (Figure 1a), with a strong normal component to the atrial surface. This may be explained by noise dominating over the intensity gradient structure present in the high-resolution images. As a result, there is

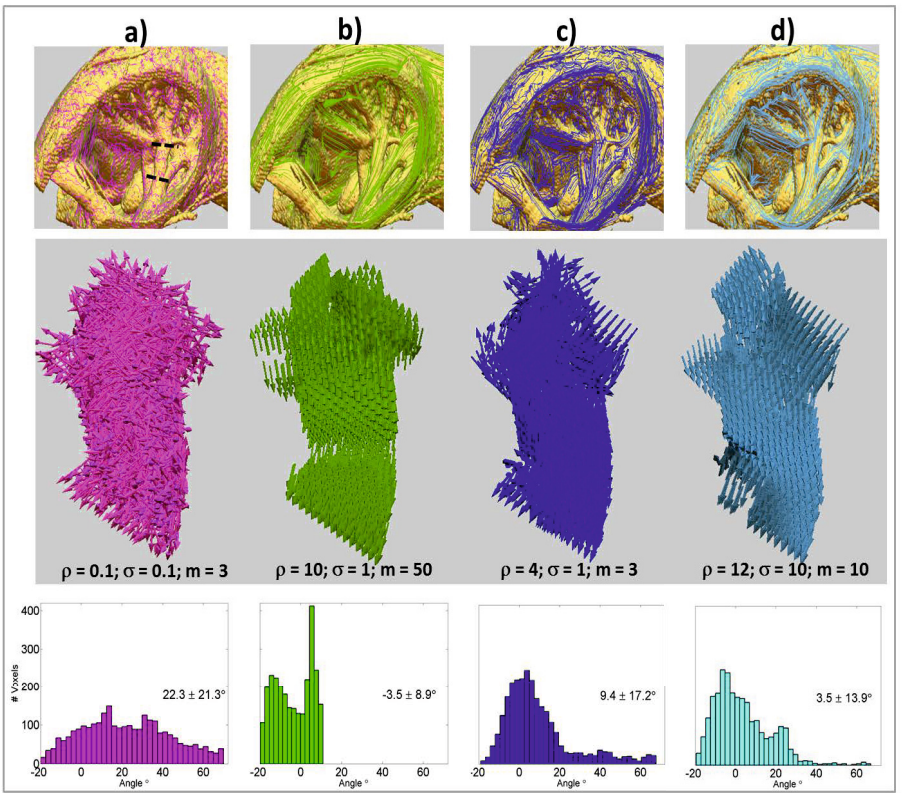

Fig. 1. Fibre orientation reconstruction in the pectinate muscle (PM) region. Reconstructions using four different sets of parameters are shown **(a-d)**. **Top:** streamline tracking of the main fibre field in the PM region, where fibres are expected to be aligned with individual PM bundles. **Middle:** arrows representing the fibre orientation field in an approximately cylindrical segment of one of the PMs (marked by dashed black lines in top panel **(a)**). **Bottom:** histograms of the angle between the fibre direction in each voxel and the main direction of the segmented PM.

a broad distribution of α across the image and fibre tracks have a wriggled non-physiological appearance. On the other hand, excessive smoothing (e.g. $\rho = 10, \sigma = 10, m = 50$) leads to a loss of local gradient information, aligning most fibre orientation vectors in an averaged direction that conveys little information about the local fibre structure (Figure 1b). As a consequence, the distribution of α is artificially narrow.

There is a range of parameters for which the fibre orientation field has physiologically realistic properties, as shown in Figures 1c and d ($\rho = 4, \sigma = 1, m = 30$ and $\rho = 12, \sigma = 10, m = 10$, respectively), with few vectors displaying a normal component to the atrial surface and relatively narrow α distributions, centred at an angle close to 0°, as most fibres are aligned with the main PM direction.

The optimal fibre orientation field parameters can be further studied by varying ρ, σ and m over a range of values. Figure 2 displays the result of such variations on the standard deviation, *std*, and mean, μ, of the fibre orientation angle distributions in the PM segment shown in the middle row of Figure 1. For m=3 (Figure 2a), both the *std* and μ of α decrease with increasing ρ and increase with increasing σ, reaching a plateau for $\rho > 3$ and $\sigma > 5$. The existence of this plateau, which can also be seen for $m = 10$ (Figure 2b), corroborates the empirical finding that there are multiple sets of parameters that produce similar fibre orientation fields. For higher values of m, the angle distribution momenta no longer reach a plateau for the σ and ρ values studied (Figure 2c).

It was found that sets of parameters that lie on the observed plateaus give the most suitable fibre orientations, avoiding under- or over-smoothing of the fibre field as seen respectively in Figures 1a and b. Therefore, a parameter set from this stable region, $\rho = 12, \sigma = 10, m = 10$, found to produce realistic fibre orientations in the PMs (Figure 1d), was used in subsequent analyses of atrial fibre orientation in this study.

Alterations in image resolution and noise levels did not affect the appearance of a plateau similar to the one displayed in Figure 2 at high values of σ and ρ and low values of m. Fibre orientation was not perceptibly affected by the addition of small amounts of noise. At high levels of noise (SNR$<$ 1) and low image resolution (512 μm), however, the observed plateau in parameter space increasingly no longer corresponded to organised fibre orientations.

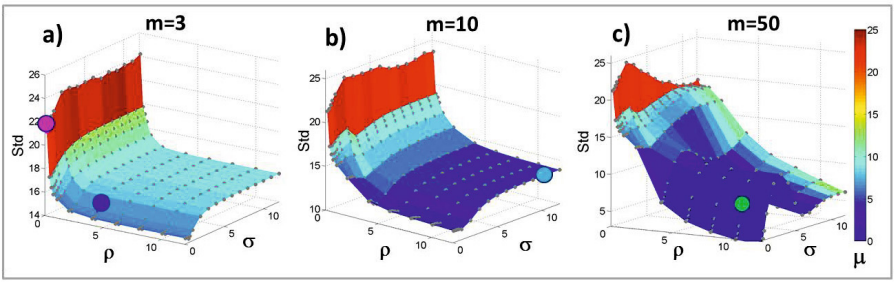

Fig. 2. Effect of image processing parameters on fibre angle distributions. Surface plots show the standard deviation, *std* (z-axis), of the distribution of the angle α between the fibre field and the main axis of the segmented PM shown in Figure 1 for different values of ρ and σ and with **a)** $m = 3$, **b)** $m = 10$ and **c)** $m = 50$. The surface colour is given by the mean, μ, of the same distribution, as indicated in the colour bar. Circles in each of the surface plots mark the position of the parameter sets used in each panel of Figure 1, using the same colour coding.

Comparison with Anatomical Studies

Streamlines of fibre tracks obtained across the whole atria with parameters $\rho = 12, \sigma = 10, m = 10$ are displayed in Figure 3. The streamlines are well aligned

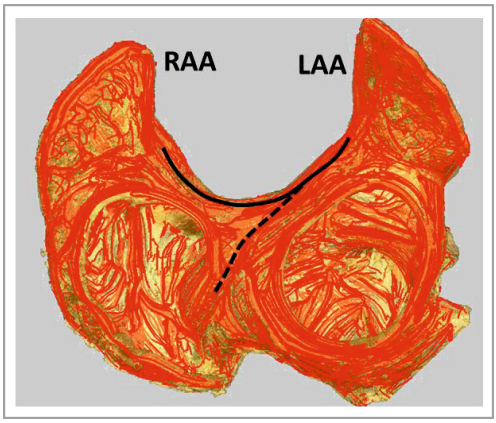

Fig. 3. Inferio-anterior view showing fibre streamlines in the whole atria. Black lines show the position of some of the main atrial bundles, as described in anatomical studies [2]. Parameters are $\rho = 12, \sigma = 10, m = 10$, as in Figure 1d, where PM fibres can be seen in more detail. Full black line: Bachmann's (interatrial) bundle; dashed black line: part of the septoatrial bundle. RAA/LAA: right/left atrial appendage.

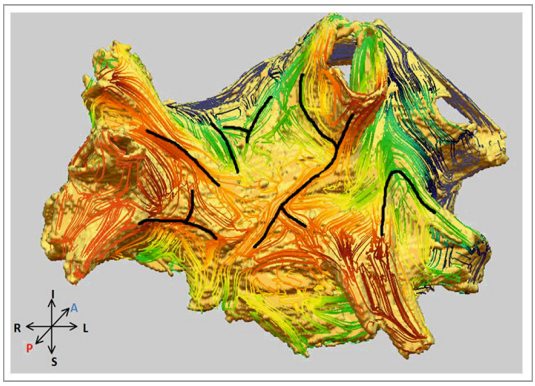

Fig. 4. Fibre streamline visualisation of the pulmonary vein sleeves and the surrounding left atrial region (posterior view). Image processing parameters, $\rho = 12, \sigma = 10, m = 10$, are the same as in Figure 1d. Streamlines are coloured according to their position in the anterior-posterior direction using a blue to red colour map. Overlying black lines show some of the main fibre orientations as described in anatomical studies [2,12].

with the main fibre directions throughout the PM area in the right atrium and along the distinctive Bachmann's and septoatrial bundles, as well as in well-defined fibres in the anterior wall of the left atrium [2].

Figure 4 shows a posterior view of the PV sleeves and the left atrium region adjacent to them using the same parameters. The fibre orientation is more disorganised, especially in the area near the PV insertions, where less well defined fibres are present [2,12]. Thick black lines showing the main fibre orientation as

described in anatomical studies [2,12] have been added to highlight the qualitative agreement between the computed fibre tracks and anatomical descriptions and also sharp changes in fibre orientation, analogous to those previously observed in histological studies [3,13,14].

4 Conclusions

In this study, we used ST analysis to obtain fibre orientation fields in the atria from high-resolution 3D micro-CT images. In the absence of a gold standard or an established theoretical framework, we used a validation method based on comparisons of the generated fibre fields in multiple well-defined atrial bundles, the PMs, where myofibres are expected to be aligned with the main fibre axis.

We found that a range of image processing parameters gave anatomically plausible fibre orientations, not only in the PM region, but also throughout the atria, in good qualitative agreement with anatomical and histological studies [2,12,3,13,14]. These optimal parameter sets were found to produce similar fibre angle distributions around the expected dominant orientation in the PM region, lying in stable plateaus in the parameter space (see Figure 2).These plateaus were stable and yielded plausible fibre orientation fields for images with SNR>1 and spatial resolution$<288\mu$m.

The micro-CT imaging method used in this study may not be suitable for *in-vivo* human imaging as it involves tissue staining and a high radiation dose. However, the investigated image processing techniques investigated can in principle be applied to any intensity-based images where there is enough contrast between myofibres and surrounding tissues, such as histological studies [15] and anatomical magnetic resonance images (MRI) [11].

Fibre orientation fields computed in the present study can be applied in simulations of biophysically detailed 3D atrial models. The generated anatomically-derived fibre fields across the whole atria allow the use of more realistic models to study action potential propagation in both physiological and pathological conditions. Atrial anisotropy, primarily in the PM and PV regions, is known to play an important role in the genesis and maintenance of AF [16]. An accurate description of the fibre orientation is therefore likely to contribute to a better understanding of the mechanisms underlying this disease.

Future work will aim to use fibre information from other modalities, such as histology or diffusion tensor MRI, DT-MRI, to provide a more rigorous validation framework for the developed methods. As DTI-MRI can estimate fibre orientation directly from water diffusion parameters and is not as time- and labour-intensive as dissection methods, it may provide a particularly good validation tool for the presented methods. The spatial resolution of DTI-MRI is, nevertheless, lower than that of micro-CT [11], making it potentially less useful for biophysical modelling applications.

Acknowledgements. This work was supported by the British Heart Foundation (PG/10/69/28524).

References

1. Lee, G., Sanders, P., Kalman, J.M.: Catheter ablation of atrial arrhythmias: state of the art. Lancet 380(9852), 1509–1519 (2012)
2. Ho, S.Y., Anderson, R.H., Sánchez-Quintana, D.: Atrial structure and fibres: morphologic bases of atrial conduction. Cardiovasc. Res. 54(2), 325–336 (2002)
3. Hocini, M., Ho, S.Y., Kawara, T., Linnenbank, A.C., Potse, M., Shah, D., Jaïs, P., Janse, M.J., Haïssaguerre, M., De Bakker, J.M.T.: Electrical conduction in canine pulmonary veins: electrophysiological and anatomic correlation. Circulation 105(20), 2442–2448 (2002)
4. Dang, L., Virag, N., Ihara, Z., Jacquemet, V., Vesin, J.M., Schlaepfer, J., Ruchat, P., Kappenberger, L.: Evaluation of Ablation Patterns Using a Biophysical Model of Atrial Fibrillation. Ann. Biomed. Eng. 33(4), 465–474 (2005)
5. Harrild, D.M., Henriquez, C.S.: A Computer Model of Normal Conduction in the Human Atria. Circ. Res. 87(7), e25–e36 (2000)
6. Krueger, M.W., Schulze, W.H.W., Rhode, K.S., Razavi, R., Seemann, G., Dössel, O.: Towards personalized clinical in-silico modeling of atrial anatomy and electrophysiology. In: Med. Biol. Eng. Comput., pp. 1–10 (2012)
7. Aslanidi, O.V., Nikolaidou, T., Zhao, J., Smaill, B.H., Gilbert, S.H., Holden, A.V., Lowe, T., Withers, P.J., Stephenson, R.S., Jarvis, J.C., Hancox, J.C., Boyett, M.R., Zhang, H.: Application of micro-computed tomography with iodine staining to cardiac imaging, segmentation, and computational model development. IEEE T. Med. Imaging 32(1), 8–17 (2013)
8. Jeffery, N.S., Stephenson, R.S., Gallagher, J.A., Jarvis, J.C., Cox, P.G.: Micro-computed tomography with iodine staining resolves the arrangement of muscle fibres. J. Biomech. 44(1), 189–192 (2011)
9. Brox, T., Van Den Boomgaard, R., Lauze, F., Van De Weijer, J., Weickert, J., Mrázek, P., Kornprobst, P.: Adaptive structure tensors and their applications. In: Visualization and Image Processing of Tensor Fields, pp. 17–47 (2006)
10. Kroon, D.-J., Slump, C.H., Maal, T.J.J.: Optimized anisotropic rotational invariant diffusion scheme on cone-beam CT. In: Jiang, T., Navab, N., Pluim, J.P.W., Viergever, M.A. (eds.) MICCAI 2010, Part III. LNCS, vol. 6363, pp. 221–228. Springer, Heidelberg (2010)
11. Gilbert, S.H., Sands, G.B., LeGrice, I.J., Smaill, B.H., Bernus, O., Trew, M.L.: A framework for myoarchitecture analysis of high resolution cardiac MRI and comparison with diffusion Tensor MRI. IEEE Eng. Med. Biol. Soc., 4063–4066 (2012)
12. Ho, S.Y., Sánchez-Quintana, D.: The importance of atrial structure and fibers. Clin. Anat. 22(1), 52–63 (2009)
13. Verheule, S., Wilson, E.E., Arora, R., Engle, S.K., Scott, L.R., Olgin, J.E.: Tissue structure and connexin expression of canine pulmonary veins. Cardiovasc. Res. 55(4), 727–738 (2002)
14. Cabrera, J.A., Ho, S.Y., Climent, V., Sánchez-Quintana, D.: The architecture of the left lateral atrial wall: a particular anatomic region with implications for ablation of atrial fibrillation. Eur. Heart J. 29(3), 356–362 (2008)
15. Zhao, J., Butters, T.D., Zhang, H., Pullan, A.J., LeGrice, I.J., Sands, G.B., Smaill, B.H.: An image-based model of atrial muscular architecture: effects of structural anisotropy on electrical activation. Circ. Arrhythm. Electrophysiol. 5, 361–370 (2012)
16. Aslanidi, O.V., Colman, M.A., Stott, J., Dobrzynski, H., Boyett, M.R., Holden, A.V., Zhang, H.: 3D virtual human atria: A computational platform for studying clinical atrial fibrillation. Prog. Biophys. Mol. Biol. 107(1), 156–168 (2011)